

Exercise restores skeletal muscle glucose delivery but not insulin-mediated glucose transport and phosphorylation in obese subjects.

Lotfi Slimani, Vesa Oikonen, Kirsti Hällsten, Nina Savisto, Juhani Knuuti, Pirjo Nuutila, Patricia Iozzo

► **To cite this version:**

Lotfi Slimani, Vesa Oikonen, Kirsti Hällsten, Nina Savisto, Juhani Knuuti, et al.. Exercise restores skeletal muscle glucose delivery but not insulin-mediated glucose transport and phosphorylation in obese subjects.: Muscle glucose metabolism in obesity and exercise. *Journal of Clinical Endocrinology and Metabolism*, Endocrine Society, 2006, 91 (9), pp.3394-403. <10.1210/jc.2006-0269>. <inserm-00402766>

HAL Id: inserm-00402766

<http://www.hal.inserm.fr/inserm-00402766>

Submitted on 8 Jul 2009

HAL is a multi-disciplinary open access archive for the deposit and dissemination of scientific research documents, whether they are published or not. The documents may come from teaching and research institutions in France or abroad, or from public or private research centers.

L'archive ouverte pluridisciplinaire **HAL**, est destinée au dépôt et à la diffusion de documents scientifiques de niveau recherche, publiés ou non, émanant des établissements d'enseignement et de recherche français ou étrangers, des laboratoires publics ou privés.

Exercise restores skeletal muscle glucose delivery but not insulin-mediated glucose transport and phosphorylation in obese subjects

Slimani Lotfi ^{1*}, Oikonen Vesa ¹, Hällsten Kirsti ¹, Savisto Nina ¹, Knuuti Juhani ¹, Nuutila Pirjo ^{1,2}, Iozzo Patricia ^{1,3}

¹ Turku PET Centre University of Turku, P.O. Box 52 20521 Turku, FI

² Department of Medicine University of Turku, Turku, FI

³ Institute of Clinical Physiology National Research Council, 56100 Pisa, IT

* Correspondence should be addressed to: Lotfi Slimani <lotfi_slimani@hotmail.com>

Abstract

Context/Objective

Insulin resistance in obese subjects results in the impaired disposal of glucose by skeletal muscle. The current study examined the effects of insulin and/or exercise on glucose transport and phosphorylation in skeletal muscle, and the influence of obesity on these processes.

Subjects/Methods

Seven obese and 12 lean men underwent positron emission tomography (PET) with 2-deoxy-2-[¹⁸F]fluoro-D-glucose ([¹⁸F]FDG) in resting and isometrically exercising skeletal muscle during normoglycemic hyperinsulinemia. Data were analyzed by two-tissue compartmental modeling. Perfusion and oxidative capacity were measured during insulin stimulation, by [¹⁵O]H₂O and [¹⁵O]O₂.

Results

Exercise increased glucose fractional uptake (K), inward transport rate (K₁) and the k₃ parameter, combining transport and intracellular phosphorylation, in lean and obese subjects. In each group, there was no statistically significant difference between plasma flow and K₁. At rest, a significant defect in K₁ (P = 0.0016), k₃ (P = 0.016) and K (P = 0.022) was found in obese subjects. Exercise restored K₁, it improved but did not normalize K (P = 0.03 vs lean), and did not ameliorate the >60% relative impairment in k₃ in obese individuals (P = 0.002 vs lean). The glucose oxidative potential tended to be reduced by obesity.

Conclusions/Interpretation

The study indicates that exercise restores the impairment in insulin-mediated skeletal muscle perfusion and glucose delivery associated with obesity, but does not normalize the defect involving the proximal steps regulating glucose disposal in obese individuals. Our data support the use of [¹⁸F]FDG-PET in the dissection between substrate supply and intrinsic tissue metabolism.

MESH Keywords Adult ; Biological Transport ; Exercise ; physiology ; Fluorodeoxyglucose F18 ; diagnostic use ; pharmacokinetics ; Glucose ; administration & dosage ; metabolism ; Humans ; Insulin ; administration & dosage ; metabolism ; Male ; Models, Biological ; Muscle Contraction ; Obesity ; metabolism ; Oxygen Consumption ; physiology ; Phosphorylation ; Positron-Emission Tomography ; Quadriceps Muscle ; blood supply ; metabolism ; radionuclide imaging ; Radiopharmaceuticals ; diagnostic use ; pharmacokinetics

Author Keywords compartmental modelling ; positron emission tomography ; [¹⁸F]FDG ; obesity ; exercise ; glucose transport and phosphorylation

Introduction

Insulin resistance in obese subjects results in an impaired use of glucose by skeletal muscle [1,2]; it is a strong predictor of the metabolic syndrome and of type 2 diabetes. In humans, insulin and exercise have synergistic increasing effects on glucose uptake [3]. Exercise strongly promotes blood flow [4] and glucose uptake regardless insulin stimulation [5,6], thus counteracting insulin resistance. In most previous studies, the actions of insulin and exercise have been studied separately [7–9]. Their simultaneous influence on skeletal muscle glucose uptake in vivo in humans has been addressed in few studies [5,10–12], but specific roles of single steps in the proximal pathway of glucose disposal were not addressed, and the confounding effect of perfusion, if any, was not separated from that of intrinsic tissue metabolism. Thus, it remains to be established whether the perfusion independent, metabolic synergy between insulin and exercise stimulation is compromised in obesity.

Dynamic positron emission tomography (PET) with 2-deoxy-2-[¹⁸F]fluoro-D-glucose ([¹⁸F]FDG) provides a non-invasive description of the tissue-specific time radioactivity curve after tracer injection, which is used for the in vivo determination of glucose transport and phosphorylation in skeletal muscle [13]. A three rate-constant (3K) model, first developed for studying the brain has been used in

estimating the first steps of glucose metabolism in the heart [14,15] and skeletal muscle [16,8,17]; it was modified by Bertoldo et al [18] to take into account the concentration of tracer in the interstitial space, by the inclusion of four compartments and five rate-constant parameters (5K model).

The compartmental model in skeletal muscle must take into account the dependency of glucose transport on blood flow and on the permeability of the sarcolemma. To simplify the model, it is assumed that [^{18}F]FDG is in equilibrium between plasma and erythrocytes [17], and that the dephosphorylation of [^{18}F]FDG-6-phosphate can be assumed to be negligible [19]. Several studies have indicated that glucose transport is the rate-limiting step for glucose uptake in skeletal muscle in normal subjects [20–23]. If the phosphorylation rate of [^{18}F]FDG is high enough to prevent any noticeable outflow of tracer from myocytes, the transport across sarcolemma is virtually irreversible. The reduced [^{18}F]FDG model for skeletal muscle can thus be described mathematically with the same three-compartmental model as for the brain (Fig. 1), albeit with a different interpretation.

The aim of the current study was to examine the *in vivo* effect of insulin and/or exercise on skeletal muscle glucose transport and phosphorylation in obese and lean subjects with dynamic PET imaging and compartmental modeling. In addition, we tested the information on skeletal muscle perfusion obtainable from [^{18}F]FDG modeling. A subset of these studies was included in a previous publication [12], addressing the question of glucose uptake *per se* by a different method. Obese and lean subjects were studied with PET in combination with [^{18}F]FDG, during insulin stimulation and one-legged exercise. Perfusion and oxygen consumption were measured with PET and [^{15}O]H₂O or [^{15}O]O₂, respectively.

Subjects, materials and methods

Subjects

Seven obese and 12 lean male untrained sedentary subjects were studied (Table 1). Maximal force of knee extensors was similar in both groups. Groups were well matched with respect to age, blood pressure, and workload during the PET study. Except for obesity, all subjects were in good general health, as judged from history, physical examination, and standard laboratory tests, and were not taking any medications. Written informed consent was obtained after nature, purpose, and potential risks of the study were explained to the subjects. The study protocol was approved by The Commission on Ethics of the University of Turku and Turku University Central Hospital.

Study design

Before the PET study, maximal oxygen uptake (VO_{2max}) and maximal isometric contractile force of the quadriceps femoris (QF) muscle were determined. The design of this study is shown in Fig. 2. Alcohol and caffeine were prohibited for 1 day before the study, and the subjects were instructed to avoid strenuous physical activity for 48 hours before the study. The PET study was performed after an overnight fast. Two catheters were inserted, one in an antecubital vein for infusion of glucose and insulin and for injection of [^{15}O]H₂O and [^{18}F]FDG, and one in the opposite radial artery for blood sampling. Muscle blood flow and oxygen consumption were measured at 60 minutes and 90 minutes after the start of insulin infusion, respectively, in both femoral regions using [^{15}O]H₂O infusion and [^{15}O]O₂ inhalation techniques, as described in detail below. At 120 minutes, a bolus of [^{18}F]FDG was injected for quantification of muscle glucose kinetics.

Exercise

All subjects were in supine position in the PET scanner with the femoral regions of both legs in the gantry and performed one-leg intermittent isometric exercise between 45 and 160 minutes (Fig. 2). Exercise consisted of two seconds of isometric knee extension in alternance with two seconds of rest.

Hyperinsulinemic clamp

At 0 minutes, an intravenous infusion of insulin at a rate of 1 mU·(kg body weight)⁻¹min⁻¹ was started. The study for each subject consisted of a 160-minute normoglycemic hyperinsulinemic period. Normoglycemia was maintained by using a variable 20% glucose infusion rate adjusted according to frequent plasma glucose concentration measurements.

Production of PET tracers

[^{18}F]FDG was synthesized with an automatic apparatus as described by Hamacher et al [24]. The specific radioactivity at the end of synthesis was 76 GBq·μmol⁻¹ with radiochemical purity > 98%. For production of [^{15}O]O₂, a low-energy deuteron accelerator Cyclone 3 was used (Ion Beam Application Inc., Louvain-la-Neuve, Belgium). [^{15}O]H₂O was produced by using a dialysis technique in a continuously working water module [25]. Sterility and pyrogenity tests were performed daily to verify the purity of the product.

Image acquisition and processing

An ECAT 931/08 PET scanner (Siemens/CTI Corp., Knoxville, TN, USA) was used for image acquisition. Each subject was positioned in the tomograph with the femoral regions in the gantry. Before emission scans, a transmission scan was performed for 20 min with a removable ring ^{68}Ge source. All data were corrected for deadtime and measured photon attenuation.

At 60 min after the start of insulin infusion, $^{15}\text{O}]\text{H}_2\text{O}$ (1.1–1.7 GBq) was injected intravenously over 30 seconds and a dynamic 6 min scan was started. To obtain the input function, arterial blood was withdrawn with a pump at a rate of 6 ml/min. Radioactivity was measured by using a two-channel detector system (Scanditronix, Uppsala, Sweden). Integrated $^{15}\text{O}]\text{H}_2\text{O}$ PET data were reconstructed by Bayesian iterative reconstruction algorithm using median root prior (MRP) [26] with 150 iterations and a Bayesian coefficient of 0.3.

For the measurement of muscle oxygen consumption, a $^{15}\text{O}]\text{O}_2$ -bolus inhalation technique was used, as validated against Fick's principle [5]. $^{15}\text{O}]\text{O}_2$ was administered at 90 min from the start of the clamp.

At 120 min, $^{18}\text{F}]\text{FDG}$ (0.15–0.33 GBq) was injected intravenously over 2 min and a 40 min dynamic scan was started (12×15 , 4×30 , 3×60 , 1×120 , and thereafter 300-s frames). Arterial blood samples for the measurement of plasma radioactivity were withdrawn during scan time, approximately one sample during each time frame. Radioactivity was assessed with an automatic gamma counter (Wizard 1480 3", Wallac, Turku, Finland). Data from $^{18}\text{F}]\text{FDG}$ images were reconstructed in a 128×128 matrix by standard algorithms with Hann filter of 0.5 cutoff frequency. The observed final in-plane resolution was 8 mm.

PET scanner and other devices for the determination of radioactivity were cross-calibrated with the automated gamma counter. Radioactivity was corrected for decay to the time of injection, and expressed in units of kBq/ml.

Regions of interest

Regions of interest (ROIs) were drawn in the anteromedial muscle compartments of both femoral regions in four consecutive cross-sectional slices, carefully avoiding large blood vessels. Localization of the muscle compartments was verified by comparing the $^{18}\text{F}]\text{FDG}$ and $^{15}\text{O}]\text{H}_2\text{O}$ images with the transmission image, which provides a topographical distribution of tissue density. The same ROIs were placed in the $^{18}\text{F}]\text{FDG}$ and $^{15}\text{O}]\text{H}_2\text{O}$ images to generate respective time-activity curves. At rest, the total volume of the regions was about 120 ml. In the exercise studies, only the ROIs on the exercising rectus femoris with the highest workload were used (~25 ml).

Perfusion analysis

For the calculation of parametric perfusion images, the autoradiographic method with an integration time of 250-s was applied. This method has been previously validated in skeletal muscle [27].

Oxygen analysis

Oxygen consumption was quantified with non-linear fitting [12]. Regional muscle oxygen uptake is given by the product of arterial oxygen concentration, regional oxygen extraction fraction and blood flow. A theoretical maximal glucose oxidative capacity was estimated based on the knowledge that 6 moles of oxygen are needed for the complete oxidation of one mole of glucose.

Compartmental modeling of $^{18}\text{F}]\text{FDG}$

Skeletal muscle $^{18}\text{F}]\text{FDG}$ time-activity curves were analyzed with a three-compartmental model [18,28–30], as shown in Fig. 1b, which comprises one extracellular (arterial plasma $^{18}\text{F}]\text{FDG}$) and two tissue compartments. Three rate constant parameters characterize the exchange of $^{18}\text{F}]\text{FDG}$ between the three compartments; K_1 ($\text{ml} \cdot \text{min}^{-1} \cdot \text{ml}^{-1}$) represents inward transport of $^{18}\text{F}]\text{FDG}$ from arterial plasma into muscle, mainly reflecting plasma flow; therefore, it is expressed in units of $\text{ml} \cdot \text{min}^{-1}$ per ml of region of interest, ROI; k_2 describes the transport rate of unphosphorylated $^{18}\text{F}]\text{FDG}$ from muscle to the venous vasculature (min^{-1}), including $^{18}\text{F}]\text{FDG}$ returning to plasma from the extracellular space because it has not been transported into myocyte and/or from the intracellular space because it has been transported into the myocyte but not phosphorylated; thus, k_2 is influenced by both K_1 and k_3 and it is not per se informative on single processes. Skeletal muscle inward transport and phosphorylation rates of $^{18}\text{F}]\text{FDG}$ are characterized by k_3 (min^{-1}). Given a high phosphorylation rate under the conditions of this study and a relatively brief duration of emission scanning [19], tracer outflow into the interstitial compartment is assumed to be negligible ($k_4 = 0$).

After administration of $^{18}\text{F}]\text{FDG}$, the total $^{18}\text{F}]\text{FDG}$ tissue concentration (C) is the sum of the free $^{18}\text{F}]\text{FDG}$ (C_E) and $^{18}\text{F}]\text{FDG-P}$ (C_M) skeletal muscle concentrations, and is expressed for each PET scan at time (t) as:

$$C(t) = C_E(t) + C_M(t)$$

This 3K model can be described mathematically by the following equations:

$$\begin{aligned} dC_E(t)/dt &= K_1 C_p(t) - [k_2 + k_3] C_E(t) & dC_E(0)/dt &= 0 \\ dC_M(t)/dt &= k_3 C_E(t) & dC_M(0)/dt &= 0 \end{aligned}$$

The model assumes that the arterial blood volume is negligible. A vascular volume V_b , representing the fraction of blood pool volume in the tissue ROI, was incorporated into the model as:

$$C_i(t) = (1 - V_b)[C_E(t) + C_M(t)] + V_b C_p(t).$$

Where C_p is the [^{18}F]FDG plasma arterial concentration.

The arterial plasma time course of [^{18}F]FDG activity C_p is used as an input function in the model. All the four model parameters K_1 , k_2 , k_3 and V_b are a priori uniquely identifiable [20].

With the use of the individual kinetic parameters, three additional combined parameters were calculated:

- – the distribution volume of non-phosphorylated extracellular [^{18}F]FDG [$DV_{CE} = K_1/k_2$, ml·ml $^{-1}$]
- – the combined transport and phosphorylation fraction (PF) of [^{18}F]FDG [$PF = k_3/(k_2 + k_3)$]
- – the fractional uptake of [^{18}F]FDG [$K = (K_1 \times k_3)/(k_2 + k_3)$, ml·ml $^{-1}$ ·min $^{-1}$]

Thus, K results in clearance units of ml·min $^{-1}$ per unit volume of region of interest, ROI. For comparison, the fractional [^{18}F]FDG uptake was estimated also by graphical methods. It was then multiplied by steady-state plasma glucose levels and divided by a LC of 1.2 to estimate skeletal muscle glucose uptake [8].

Parameter estimation

All kinetic parameters were determined by iterative curve fitting and the minimization of an objective function implemented in the SAAM II software [31]. Compartmental model parameters were estimated by weighted nonlinear least squares and the measured PET activity, C^{obs} , was described as:

$$C^{obs}(t_j) = C(t_j) + e(t_j) \quad j = 1, 2 \dots N$$

where $e(t_j)$ is the measurement error at time t_j assumed to be independent, Gaussian, zero mean. The parameters precision was judged by the residual error evaluation calculated at the different sample time as:

$$wres_{ij} = \sqrt{w_{i,j}} [s(\hat{p}, t_{ij}) - y_{i,j}]^2$$

where $w_{i,j}$ is the weight associated with each datum, $s(\hat{p}, t_{ij})$ is the value predicted by the model, $y_{i,j}$ is the measured experimental value and p is the unknown parameter estimated. SAAM II calculates a weight “ $w_{i,j}$ ” associated with each datum “ $y_{i,j}$ ” from the standard deviation that has been assigned to the datum by the user, a fractional standard deviation (FSD) of “0.1” was assigned to each datum.

Statistical analysis

Results are expressed as mean \pm SD. Values of model parameters with low precision, as defined by a coefficient of variation ($CV = SD(\hat{p}_i)/\hat{p}_i \times 100$, where \hat{p}_i is the parameter estimate and $SD(\hat{p}_i)$ is its standard deviation) $>100\%$ were excluded from the calculation of the group mean. Data comparison was determined by using the Student's t test. Correlations and linear regression were used to examine associations between variables. A $p < 0.05$ was considered to be significant. Statistical analysis was performed using Statview for Windows, SAS institute.

Results

Metabolic characteristics

Clinical and biochemical characteristics of the groups are shown in Table 1. Fasting serum insulin concentrations were slightly higher in obese than in lean subjects, whereas fasting plasma glucose concentrations were similar (5.3 ± 0.2 vs 5.4 ± 0.2 mmol·L $^{-1}$). Maximal aerobic capacity ($VO_{2,max}$) was significantly higher in lean than in obese subjects ($p < 0.01$).

Compartmental modeling

A representative example of the measured plasma and muscle activity curves for subject 4 (lean) at rest and during exercise is shown in Fig. 3a. The shape of the [^{18}F]FDG activity curves documented faster tracer uptake during exercise. Model parameters were estimated with good precision in most studies; individual results are shown in Tables 2–3.

Simulation

The 3K model was able to predict the time course of tracer concentrations in each compartment. An example is given in Fig. 3, delineating model predicted time activity curves of extracellular (q_2), intracellular and phosphorylated [^{18}F]FDG (q_3) in subject 4, showing an increase in q_3 in exercising (Fig. 3b) as compared with resting skeletal muscle (Fig. 3c).

Effects of insulin and exercise

The rate constant for [^{18}F]FDG transport from the extracellular compartment into tissue (K_1) showed a significant increase during exercise ($p < 0.01$) in lean subjects (Tables 2–3); a 3.5 fold stimulation was observed in obese individuals ($p < 0.014$) (Tables 2–3). A significant difference between rest and exercise was observed in the [^{18}F]FDG outward transport parameter, k_2 , in lean subjects ($p < 0.05$). The distribution of k_2 values covered a wide range and was slightly skewed, with median values of 0.191 and 0.141 min^{-1} (141 and 107% of the mean) in obese individuals during exercise and rest, respectively, as compared with 0.554, and 0.322 min^{-1} in lean subjects (92 and 97% of mean, respectively). Exercise determined a more than three fold increase in k_3 in lean and obese subjects ($p < 0.001$). Exercise increased PF (0.469 ± 0.248 and 0.707 ± 0.265 , $p < 0.05$) in lean, but not in obese subjects. It did not affect DV_{CE} . Estimated values for the vascular volume, V_b , were 3-fold and 5-fold higher in lean and obese individuals, respectively, in the exercising than in the resting leg ($p < 0.0001$).

Lean vs obese subject

Parameter comparison between lean and obese subjects are shown in Fig. 4(a–e). In resting skeletal muscle, K_1 , representing blood flow and substrate delivery in skeletal muscle (Fig. 4a), was 2.5 fold higher ($p < 0.01$), k_3 (transport and phosphorylation) was 3 fold higher ($p < 0.05$) (Fig. 4c) and K (fractional uptake, Fig. 4d) was 2 times higher in lean than in obese subjects ($p < 0.05$). In exercising skeletal muscle, k_2 was 4-fold higher ($p < 0.01$), and k_3 was significantly higher in lean than obese subjects ($p < 0.01$). The fractional uptake of [^{18}F]FDG was 79% higher in lean as compared with obese subjects ($p < 0.05$).

Blood flow

Plasma flow values were calculated from blood flow PET data, by using the hematocrit. There was no significant difference between plasma flow and K_1 values estimated by [^{18}F]FDG compartmental modeling (Fig. 4a), though the correlation between individual values did not reach statistical significance.

Modelling vs graphical analysis

The rate constant, K , reflecting the net utilization of [^{18}F]FDG from the arterial compartment into skeletal muscle was estimated by both 3K modeling and Gjedde-Patlak graphical analysis [32,33]. We found a strong correlation between these two methods ($p < 0.0001$, $R^2 = 0.96$) in each group (obese and lean) and in both resting and exercising legs (Fig. 5). No correlation was found between K and individual parameters derived by 3K modeling.

Oxidative capacity

The maximal glucose oxidative potential was significantly increased by exercise in both groups (lean subjects 16 ± 3 vs 277 ± 40 $\mu\text{mol} \cdot \text{kg}^{-1} \cdot \text{min}^{-1}$ in resting and exercising leg, $p = 0.0002$; obese subjects 12 ± 3 vs 200 ± 40 $\mu\text{mol} \cdot \text{kg}^{-1} \cdot \text{min}^{-1}$, respectively, $p = 0.005$). During exercise, a tendency towards defective glucose oxidative potential was observed in obese vs lean subjects, which fell short of statistical significance ($p = 0.2$).

Discussion

The main results of the present study indicate that skeletal muscle perfusion, glucose transport and phosphorylation defects are concomitant findings in obesity during insulin-stimulation, and that, by restoring perfusion but not the proximal metabolic steps of glucose disposal, exercise unravels the predominance of the metabolic impairment in the obese population. To the best of our knowledge, this is the first report describing the combined effects of exercise and insulin stimulation on skeletal muscle glucose kinetics, as analysed by compartmental modeling of PET data. Under euglycemic hyperinsulinemia, exercise enhanced skeletal muscle perfusion to a similar extent in lean and obese subjects, but did not ameliorate the relative defect in glucose transport and phosphorylation. The oxidative capacity tended to be lower in obese subjects during exercise.

The 3K modeling of dynamic [^{18}F]FDG data used in our study has been adopted to quantify glucose metabolism rates in skeletal muscle in humans by other authors [13–15]. Recently, Bertoldo et al have proposed a four-compartment model with five parameters (5K model) [20], which enable dissection of glucose transport and phosphorylation. This model was applied by Williams et al [34,35], revealing that insulin resistance involves both metabolic processes in obesity and type 2 diabetes. The reduced 3K model used in our study has been

shown to provide accurate fits to muscle data both in fasting and insulin stimulated conditions [8,17]. Reinhardt et al [17] tested the 3-compartment model (3K model) against more reduced 2-compartment model and complex (4-compartment model) approaches, by using the Akaike and Schwarz information criteria; their results favored the present reduced model, suggesting that the fourth compartment, i.e., phosphorylated [¹⁸F]FDG cannot be clearly identified from [¹⁸F]FDG kinetics in the skeletal muscle, especially given a relatively limited study duration [17], similar to that in the present design. Given the overall study length required for the sequence of measurements performed here after the achievement of metabolic steady-state, we opted for a 40 min [¹⁸F]FDG PET scanning time, and we cannot exclude that a prolonged experiment may have been compatible with a more complex and informative model, as described by others [20]. In our hands, the current model permitted a good estimation and unique identification of parameters in most subjects in both groups, with few exceptions, due to the original data quality.

We confirm the previous observation of an impaired glucose uptake in obese vs lean subjects both in resting and exercising muscle, and showed a strong correlation between compartmental modeling and linearly derived fractional [¹⁸F]FDG uptake values in all study groups and conditions. In our previous report, skeletal muscle glucose uptake rates in a subgroup of this population have been estimated by using graphical methods [32,33]. These methods do not allow resolve between flow and metabolic modulation of the target process. Since the influence of glucose delivery on glucose uptake remains a matter of debate [36], and it may vary upon study population and conditions, it was not possible to define to which extent an intrinsic metabolic process was responsible for the observed defect. The lack of a correlation between glucose uptake and the individual inward parameters of the model in this study underlines this limitation, and its inter-subject dependency. Notably, the current analysis method contributes a relevant piece of information, in that it allows almost fully separate the effect of perfusion and substrate delivery from the intrinsic ability of the tissue to transport and phosphorylate glucose. The evidence of reduced insulin-mediated perfusion in obesity in resting skeletal muscle has been previously reported [37], and it concordantly resulted from two independent methods in the current study, in which the use of PET allowed selectively target skeletal muscle with no influence of surrounding structures. The parameter k_3 is interpreted as described by other authors [12,13,15,34] as an aggregate parameter reflecting both skeletal muscle glucose transport and intracellular phosphorylation. The rate of this process was decreased by approximately 65 and 62% in resting and exercising muscle, respectively, in obese as compared with lean subjects, in spite of a significant effect of exercise in promoting both perfusion and glucose transport and phosphorylation in both study groups during euglycemic hyperinsulinemia. Therefore, skeletal muscle insulin resistance is associated with an impaired response of the proximal steps responsible for the metabolic disposal of glucose in obese subjects, due to an intrinsic tissue defect, which persists with similar severity during exercise stimulation. In fact, the k_3 difference between groups unparalleled that in tissue perfusion, which was impaired at rest and restored during exercise, documenting the independency of the intrinsic component of insulin resistance from substrate delivery in obese subjects during exercise. A single bout of exercise has been long recognized to enhance insulin mediated whole body glucose uptake [3,5], an effect that is protracted for several subsequent hours; consequently, exercise has been considered as one cornerstone of treatment in insulin resistant conditions. Although confirming that acute exercise strongly accelerates the rate of glucose entry in skeletal muscle, more than doubling the effect of insulin stimulation in lean and obese individuals, our data document that such stimulation does not normalize this process, thus, perpetuating the same >60% defect in muscle glucose transport and phosphorylation in obese patients. Notably, our results refer to a single bout exercise in untrained individuals, and cannot be directly extrapolated to the case of regular training or of single bout exercise in trained subjects. Moreover, because glucose disposal results from the fractional uptake rate, which is a composite parameter accounting for perfusion and transport/phosphorylation (in graphical analysis) or K_1 and k_3 (in the 3K model), the above considerations are not to be taken as to indicate that exercise does not alleviate insulin resistance in obesity. However, they indicate that K_1 , rather than k_3 was responsible for a less than 20% reduction in the relative fractional uptake gap between lean and obese subjects in our study. Accordingly, k_2 was up-regulated during exercise, and higher in lean than obese individuals; this parameter showed inter-individual variability, partly because it reflects a balance of several processes (see methods), among which perfusion appeared to be predominant in our study.

The obesity related defect in glucose transport and phosphorylation, has been interpreted as being of a secondary origin, as it was reversed by weight reduction [34]. Extrapolating from our previous and current findings, we calculated a theoretical maximum glucose oxidation rate, by assuming that all oxygen extracted by skeletal muscle was utilized for the oxidation of this substrate. Under conditions of insulin stimulation, such as in the present study, circulating fatty acids are suppressed, and their storage in complex lipids is favored. Thus, glucose is the main fuel undergoing oxidation, the latter process accounting for approximately 30% of glucose uptake in healthy individuals [38]. Consistent with this knowledge, the glucose oxidative capacity in healthy subjects was on average $16 \mu\text{mol}\cdot\text{min}^{-1}\cdot\text{kg}^{-1}$ in resting skeletal muscle, corresponding to $28 \pm 5\%$ of glucose uptake in this organ; it was enhanced by approximately 15-fold in both groups in the exercising situation, thus exceeding the disposal of plasma glucose, suggesting internal storage breakdown. A tendency towards a lower glucose oxidative capacity in obese subjects was observed, falling short of statistical significance during exercise. Given the more pronounced reduction in glucose uptake than oxidative potential in obese subjects, the above evidence may indicate that either a larger proportion of delivered glucose is oxidized leading to a deficient glycogen incorporation or, more likely, the oxidation of alternative substrates or fuel sources operates to compensate for the limited availability of glucose in these individuals in this high energy requiring condition.

The first step of glucose uptake in tissue is the delivery by perfusion, which was shown here to be relevant in regulating the synergy between exercise and insulin in obese subjects. One salient finding of this study was that in each group and experimental condition, we observed no significant difference between plasma flow, as estimated from [^{15}O]H $_2$ O PET analysis and the [^{18}F]FDG inward rate constant K_1 . Mean values in lean subjects were 2.5 vs 3.1 in the resting leg, and 5.6 vs 5.5 ml·100g $^{-1}$ min $^{-1}$ in the exercising leg, respectively by the two methods; corresponding figures in obese subjects were 1.1 vs 1.2 and 3.1 vs 4.3 ml·100g $^{-1}$ min $^{-1}$.

The current results are consistent with estimated K_1 values in previous [^{18}F]FDG PET studies, and similar to the known perfusion rates of 2–4 ml·100g $^{-1}$ min $^{-1}$ in resting skeletal muscle [39]. After unit conversion, published values ranged between 1.1–5 and 0.6–2.2 ml·100g $^{-1}$ min $^{-1}$ in resting skeletal muscle in lean and obese subjects, respectively [7,8,16,17]. A significant correlation between leg blood flow and K_1 has been previously reported [8], suggesting an influence of tissue perfusion on K_1 . In spite of the above evidence, K_1 has been variably interpreted as predominantly reflecting glucose transport [8] or blood flow [34]. The former concept was inherited from the original application of the reduced 3K model to the quantification of brain glucose uptake, where a) the capillary endothelium forms a tight blood-brain barrier and is rate-limiting for glucose transport, thus, the interstitial space and intracellular space can be combined in one compartment [28,29], and b) the permeability surface area product (PS) is \ll blood flow, and the transport of glucose to tissue is nearly independent of blood flow, thus, the effect of blood flow has been eliminated in the model [28,29]. By converse, in skeletal muscle, a) the capillary wall allows free diffusion of small hydrophilic solutes [40], and the sarcolemma becomes more rate-limiting for the transport of glucose than the endothelium, and b) the PS for glucose is approximately 5 ml·100g $^{-1}$ min $^{-1}$ [40] and is in the same order of magnitude as blood flow [39], which represents one further rate limiting factor in this tissue. The equivalence between K_1 , i.e., the first rate limiting parameter in the model, and the [^{15}O]H $_2$ O derived tissue perfusion in this and previous studies is in keeping with the above knowledge. Our finding demonstrates that modelling of [^{18}F]FDG can be used as a reliable surrogate for the evaluation of skeletal muscle perfusion, as previously surmised [34], also incorporating the influence of trans-endothelial diffusion, thus reflecting the integrated process of substrate delivery. In PET scanning, the assessment of perfusion needs to precede that of glucose uptake by at least 15 minutes. Because insulin action is time dependent, the lack of simultaneity unpredictably affects the evaluation of the glucose extraction fraction. This, together with the influence of trans-endothelial transport on K_1 likely explains the lack of a correlation against [^{15}O]H $_2$ O measurements in our study. Thus, [^{18}F]FDG modelling provides simultaneous information on intrinsic glucose metabolism and substrate delivery (including perfusion and endothelial transport) in skeletal muscle.

In summary, the current study showed that, under insulin stimulated conditions, exercise promotes skeletal muscle perfusion and glucose transport/phosphorylation in lean and obese subjects, it restores the impairment in muscle perfusion associated with obesity, but does not normalize the defect involving the proximal steps regulating skeletal muscle glucose disposal in obese individuals. Oxidative and non-oxidative glucose metabolic defects likely co-exist in skeletal muscle, under combined exercise and insulin stimulation in these subjects. Our data support the use of [^{18}F]FDG-PET in the evaluation of skeletal muscle perfusion and glucose delivery, and in the dissection between the substrate supply and the inherent metabolic dependency of insulin resistance in skeletal muscle.

Acknowledgements:

This study was supported by grants from the Academy of Finland (203958 to P.I., 206359 to P.N.), the Novo Nordisk Foundation, the Sigrid Juselius Foundation, the Finnish Diabetes Foundation (to P.I.) and Research Society, and the Turku University Foundation (to P.I.). We are grateful to the staff of the Turku PET Centre for their excellent technical assistance.

Abbreviations

PET: positron emission tomography

[^{18}F]FDG: 2-deoxy-2-[^{18}F]fluoro-D-glucose

References:

1. Campbell PJ, Carlson MG 1993; Impact of obesity on insulin action in NIDDM. *Diabetes*. 42: (3) 405- 10
2. Ludvik B, Nolan JJ, Baloga J, Sacks D, Olefsky J 1995; Effect of obesity on insulin resistance in normal subjects and patients with NIDDM. *Diabetes*. 44: (9) 1121- 5
3. DeFronzo RA, Ferrannini E, Sato Y, Felig P, Wahren J 1981; Synergistic interaction between exercise and insulin on peripheral glucose uptake. *J Clin Invest*. 68: (6) 1468- 74
4. Dela F, Mikines KJ, Sonne B, Galbo H 1994; Effect of training on interaction between insulin and exercise in human muscle. *J Appl Physiol*. 76: (6) 2386- 93
5. Nuutila P, Peltoniemi P, Oikonen V, Larmola K, Kempainen J, Takala T, Sipila H, Oksanen A, Ruotsalainen U, Bolli GB, Yki-Järvinen H 2000; Enhanced stimulation of glucose uptake by insulin increases exercise-stimulated glucose uptake in skeletal muscle in humans: studies using [^{15}O]O $_2$, [^{15}O]H $_2$ O, [^{18}F]fluoro-deoxy-glucose, and positron emission tomography. *Diabetes*. 49: (7) 1084- 91
6. Peltoniemi P, Lonroth P, Laine H, Oikonen V, Tolvanen T, Gronroos T, Strindberg L, Knuuti J, Nuutila P 2000; Lumped constant for [(18)F]fluorodeoxyglucose in skeletal muscles of obese and nonobese humans. *Am J Physiol Endocrinol Metab*. 279: (5) E1122- 30
7. Kelley DE, Mintun MA, Watkins SC, Simoneau JA, Jadali F, Fredrickson A, Beattie J, Thériault R 1996; The effect of non-insulin-dependent Diabetes Mellitus and obesity on glucose transport and phosphorylation in skeletal muscle. *J Clin Invest*. 97: 2705- 2713
8. Kelley DE, Williams KV, Price JC 1999; Insulin regulation of glucose transport and phosphorylation in skeletal muscle assessed by PET. *Am J Physiol*. 277: E361- E369
9. Williams KV, Price JC, Kelley DE 2001; Interactions of impaired glucose transport and phosphorylation in skeletal muscle insulin resistance: a dose-response assessment using positron emission tomography. *Diabetes*. 50: (9) 2069- 79

- 10. Nuutila P, Kalliokoski K 2000; Use of positron emission tomography in the assessment of skeletal muscle and tendon metabolism and perfusion. *Scand J Med Sci Sports*. 10: (6) 346- 50
- 11. Peltoniemi P, Yki-Järvinen H, Oikonen V, Oksanen A, Takala TO, Ronnema T, Erkinjuntti M, Knuuti MJ, Nuutila P 2001; Resistance to exercise-induced increase in glucose uptake during hyperinsulinemia in insulin-resistant skeletal muscle of patients with type 1 diabetes. *Diabetes*. 50: (6) 1371- 7
- 12. Hällsten K, Yki-Järvinen H, Peltoniemi P, Oikonen V, Takala T, Kemppainen J, Laine H, Bergman J, Bolli GB, Knuuti J, Nuutila P 2003; Insulin- and exercise-stimulated skeletal muscle blood flow and glucose uptake in obese men. *Obes Res*. 11: (2) 257- 65
- 13. Mossberg KA, Taegtmeyer H 1992; Time course of skeletal muscle glucose uptake during euglycemic hyperinsulinemia in the anesthetized rabbit: a fluorine-18-2-deoxy-2-fluoro-D-glucose study. *J Nucl Med*. 33: (8) 1523- 9
- 14. Marshall RC, Powers-Risius P, Huesman RH, Reutter BW, Taylor SE, Maurer HE, Huesman MK, Budinger TF 1998; Estimating glucose metabolism using glucose analogs and two tracer kinetic models in isolated rabbit heart. *Am J Physiol*. 275: (2 Pt 2) H668- 79
- 15. Yokoyama I, Ohtake T, Momomura S, Yonekura K, Kobayakawa N, Aoyagi T, Sugiura S, Yamada N, Ohtomo K, Sasaki Y, Omata M, Yazaki Y 1999; Insulin action on heart and skeletal muscle FDG uptake in patients with hypertriglyceridemia. *J Nucl Med*. 40: (7) 1116- 21
- 16. Selberg O, Burchert W, van den Hoff J, Meyer GJ, Hundeshagen H, Radoch E, Balks HJ, Müller MJ 1993; Insulin resistance in liver cirrhosis: positron-emission tomography scan analysis of skeletal muscle glucose metabolism. *J Clin Invest*. 91: 1897- 1902
- 17. Reinhardt M, Beu M, Vosberg H, Herzog H, Hübinger A, Reinauer H, Müller-Gärtner HW 1999; Quantification of glucose transport and phosphorylation in human skeletal muscle using FDG PET. *J Nucl Med*. 40: 977- 985
- 18. Bertoldo A, Peltoniemi P, Oikonen V, Knuuti J, Nuutila P, Cobelli C 2001; Kinetic modeling of [(18)F]FDG in skeletal muscle by PET: a four-compartment five-rate-constant model. *Am J Physiol Endocrinol Metab*. 281: (3) E524- 36
- 19. Lackner R, Challiss RA, West D, Newsholme EA 1984; A problem in the radiochemical assay of glucose-6-phosphatase in muscle. *Biochem J*. 218: 649- 651
- 20. Roussel R, Carlier PG, Robert JJ, Velho G, Bloch G 1998; ¹³C/³¹P NMR studies of glucose transport in human skeletal muscle. *Proc Natl Acad Sci USA*. 95: 1313- 1318
- 21. Cline GW, Petersen KF, Krssak M, Shen J, Hundal RS, Trajanoski Z, Inzucchi S, Dresner A, Rothman DL, Shulman GI 1999; Impaired glucose transport as a cause of decreased insulin-stimulated muscle glycogen synthesis in type 2 diabetes. *N Engl J Med*. 341: 240- 246
- 22. Katz A, Nyomba BL, Bogardus C 1985; No accumulation of glucose in human skeletal muscle during euglycemic hyperinsulinemia. *Am J Physiol*. 255: E942- E945
- 23. Fink RI, Wallace P, Brechtel G, Olefsky JM 1992; Evidence that glucose transport is rate-limiting for in vivo glucose uptake. *Metabolism*. 41: 897- 902
- 24. Hamacher K, Coenen HH, Stöcklin G 1986; Efficient stereospecific synthesis of no-carrier added 2-[¹⁸F]-fluoro-2-deoxy-D-glucose using aminopolyether supported nucleophilic substitution. *J Nucl Med*. 27: 235- 238
- 25. Crouzel C, Clarc J, Brihaye C, Långström B, Lemaire C, Meyer G, Nebeling B, Stone-Elander S Editor: Stöcklin G, Pike V 1993; Radiochemistry automation in PET. *Radiopharmaceuticals for Positron Emission Tomography*. Dordrecht, The Netherlands Kluwer Academic Publisher Group; 45- 90
- 26. Alenius S, Ruotsalainen U 1997; Bayesian image reconstruction for emission tomography based on median root prior. *Eur J Nucl Med*. 24: 258- 265
- 27. Ruotsalainen U, Raitakari M, Nuutila P, Oikonen V, Sipilä H, Teräs M, Knuuti J, Bloomfield PM, Iida H 1997; Quantitative blood flow measurement of skeletal muscle using oxygen-15-labeled water and PET. *J Nucl Med*. 38: 314- 319
- 28. Phelps ME, Huang SC, Hoffman EJ, Selin C, Sokoloff L, Kuhl DE 1979; Tomographic measurement of local cerebral glucose metabolic rate in humans with (F-18)2-fluoro-2-deoxy-D-glucose: Validation of method. *Ann Neurol*. 6: 371- 388
- 29. Huang SC, Phelps ME Editor: Phelps M, Mazziotta J, Schelbert H 1986; Principles of tracer kinetic modeling in positron emission tomography and autoradiography. Principles and applications for the brain and heart. Raven Press; New York 287- 346
- 30. Sokoloff L, Reivich M, Kennedy C, Des Rosiers MH, Patlak CS, Pettigrew KD, Sakurada O, Shinohara M 1977; The [14C]deoxyglucose method for the measurement of local cerebral glucose utilization: theory, procedure, and normal values in the conscious and anesthetized albino rat. *J Neurochem*. 28: (5) 897- 916
- 31. SAAM Institute 1998; SAAM II User's guide version 1.1.1. Seattle, WA SAAM Institute;
- 32. Gjedde A, Diemer NH 1983; Autoradiographic determination of regional brain glucose content. *J Cereb Blood Flow Metab*. 3: 330- 310
- 33. Patlak CS, Blasberg RG 1985; Graphical evaluation of blood-to-brain transfer constants from multiple-time uptake data. Generalizations. *J Cereb Blood Flow Metab*. 5: 584- 590
- 34. Williams KV, Bertoldo A, Kinahan P, Cobelli C, Kelley DE 2003; Weight loss-induced plasticity of glucose transport and phosphorylation in the insulin resistance of obesity and type 2 diabetes. *Diabetes*. 52: (7) 1619- 26
- 35. Williams KV, Bertoldo A, Mattioni B, Price JC, Cobelli C, Kelley DE 2003; Glucose transport and phosphorylation in skeletal muscle in obesity: insight from a muscle-specific positron emission tomography model. *J Clin Endocrinol Metab*. 88: (3) 1271- 9
- 36. Wasserman DH, Ayala JE 2005; Interaction of physiological mechanisms in control of muscle glucose uptake. *Clin Exp Pharmacol Physiol*. 32: (4) 319- 23
- 37. Shoemaker JK, Bonen A 1995; Vascular actions of insulin in health and disease. *Can J Appl Physiol*. 20: (2) 127- 54
- 38. Ferrannini E, DeFronzo RA Editor: Alberti KGMM, Zimmet P, DeFronzo RA, Keen H 1997; Insulin actions in vivo: glucose metabolism. John Wiley & Sons; International Textbook of Diabetes Mellitus. 505- 529
- 39. Ganong WF 1995; Review of Medical Physiology. Appleton & Lange; 17
- 40. Crone C, Levitt DG 1984; Capillary permeability to small solutes. Handbook of physiology. The cardiovascular system. Microcirculation. Am Physiol Soc; Bethesda, MD IV: (1) 411- 466

FIG. 1

a: The uptake of [^{18}F]FDG consists of several steps: delivery to the tissue by arterial blood flow; diffusion from plasma in vascular to interstitial space over the capillary wall, facilitative transport from interstitial space to intracellular space via glucose transporters, and phosphorylation by hexokinase in the intracellular space. The dashed and dotted boxes indicate the compartments that are combined in the present reduced model (8). b: In the current model, the interstitial and intracellular [^{18}F]FDG spaces are approximated to a single compartment C_2 , and the capillary concentration is approximated to the measured arterial plasma (C_A) (6); K_1 represents inward transport of [^{18}F]FDG from arterial plasma into muscle, mainly reflecting plasma flow, thus, it is conventionally expressed in units of ml/min per unit of tissue region of interest, ml ROI; k_2 describes the transport rate of unphosphorylated [^{18}F]FDG from muscle to the venous vasculature, and k_3 is the rate constant regulating skeletal muscle inward transport and phosphorylation of [^{18}F]FDG; k_4 is assumed to be negligible.

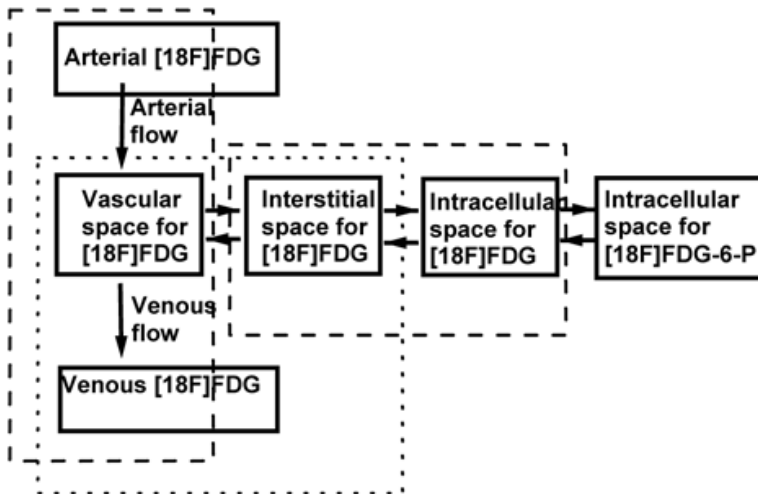
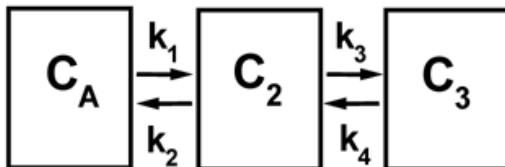
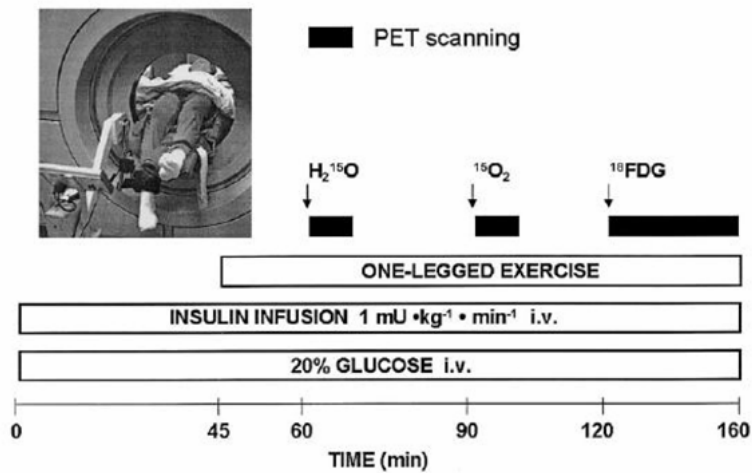
a**b**

FIG. 2

Study design. Insulin was infused intravenously at a rate of 1 mU/kg per minute, and glucose was infused intravenously to maintain normoglycemia. The insert shows the setup of the one-legged exercise, which consisted of intermittent isometric contractions. [^{15}O]H $_2\text{O}$ (i.v. bolus), [^{18}F]FDG (i.v. bolus) and [^{15}O]O $_2$ (by inhalation) were administered to quantify rates of blood flow, oxygen consumption, and glucose uptake simultaneously in the resting and exercising legs during euglycemic hyperinsulinemia; black boxes indicate the duration of each PET acquisition.

**FIG. 3**

Example of compartmental model fit to the measured tissue activity curves in one lean subject (number 4), showing a good agreement between estimated (continuous lines) and measured values (squares). Top panel a: Model interpolation of plasma activity was used as a forcing function. Bottom panels b and c: Model estimate (continuous lines) and measured tissue data (squares) obtained in skeletal muscle in exercising (left panel b) and resting legs (right panel c), where line s_2 represents the model fit to total tissue radioactivity over time, and lines q_2 and q_3 are model simulations of free and phosphorylated [^{18}F]FDG concentrations in tissue compartments 2 and 3 (C2 and C3 in Fig. 2).

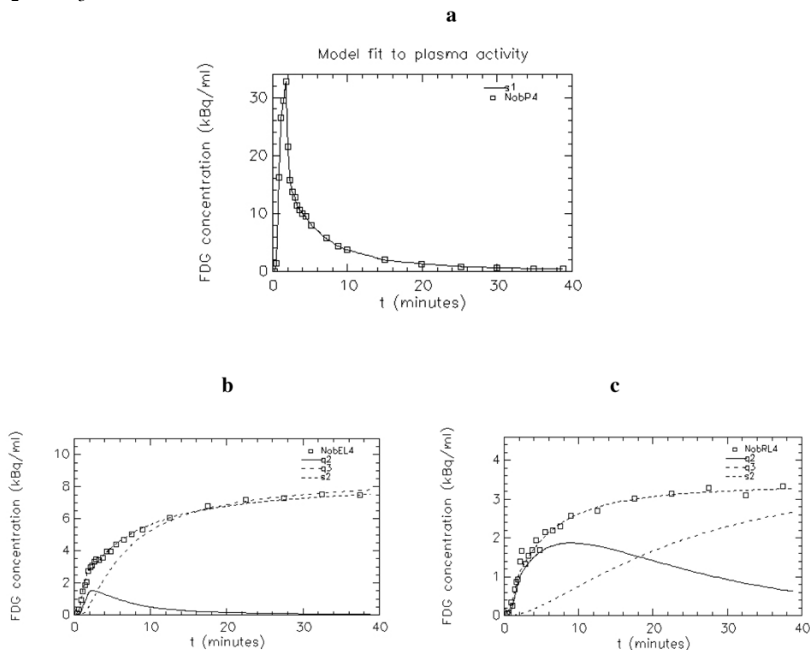
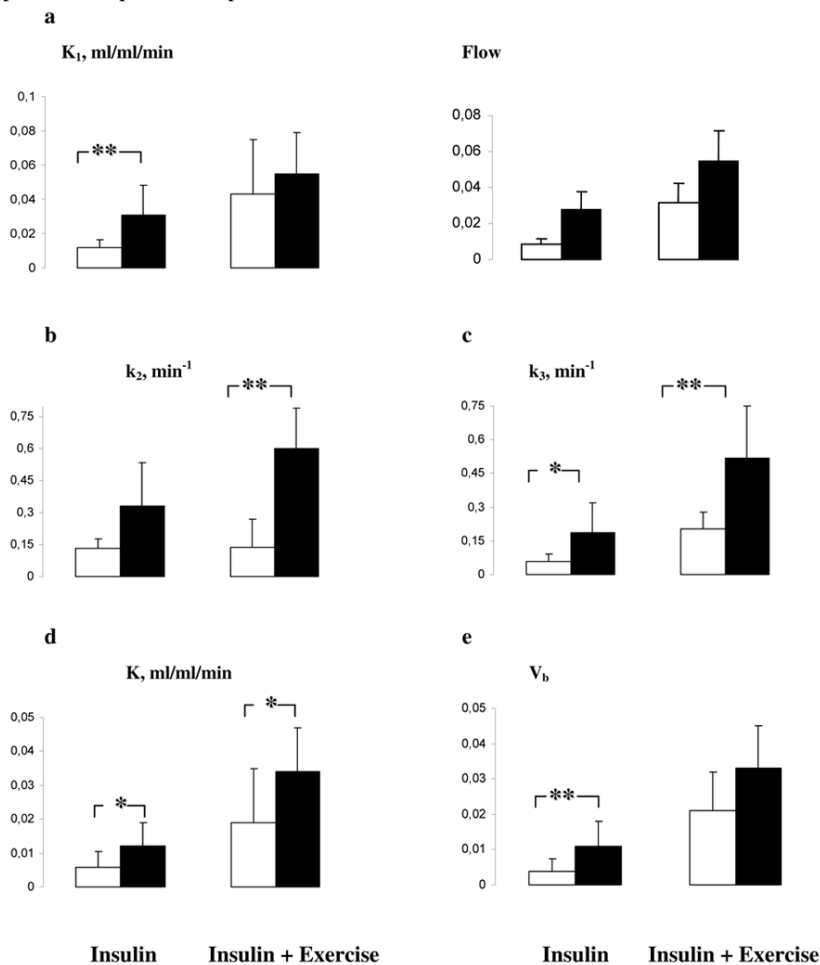


FIG. 4

Model estimated glucose rate constants (a–e) in obese (white bars) and lean subjects (black bars) during euglycemic hyperinsulinemia ± exercise. In the top right panel, [¹⁵O]H₂O-determined plasma flow is shown to enable its comparison with the [¹⁸F]FDG-determined K₁ parameter. *p < 0.05; **p < 0.01.

**FIG. 5**

Linear regression between K_i values, as estimated by graphical analysis and calculated by using the 3K model derived parameters.

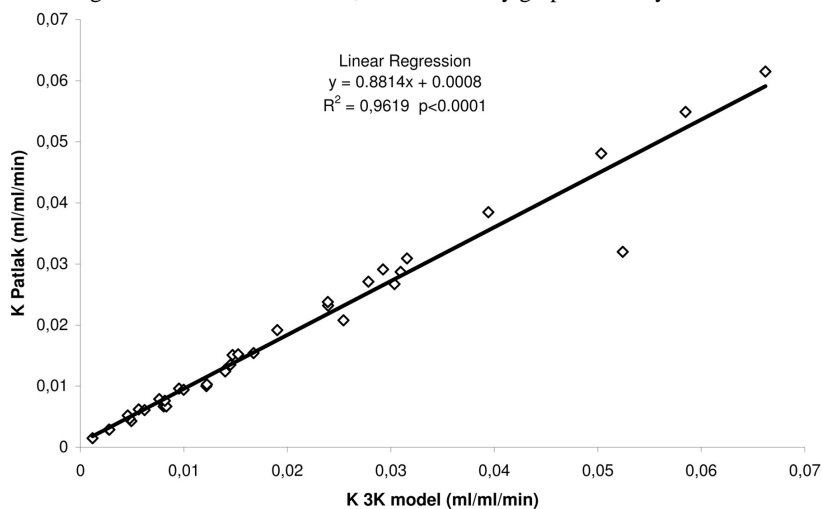


TABLE 1

Clinical and biochemical characteristics of the subjects

	Lean	Obese
n	12	7
Age (years)	24 ± 2	29 ± 6
Weight (kg)	72.6 ± 6	123.8 ± 16 [†]
Body mass index (kg/m ²)	22 ± 2	35.6 ± 5 [†]
Mean percent of body fat (%)	15.8 ± 5	28.8 ± 1 [†]
Fasting plasma glucose (mM)	5.3 ± 0.2	5.4 ± 0.2
Fasting serum insulin (mU/L)	6.2 ± 2	15.6 ± 4 [*]
Maximal isometric force (N)	608 ± 124	718 ± 198
Work force during exercise (N)	85.7 ± 13	85.9 ± 9
VO ₂ max (ml/kg BW/min)	50.8 ± 10	31.4 ± 4 [*]

Data are means ± SE.

^{*} p < 0.01 and[†] p < 0.001. N, Newton. BW, body weight.

TABLE 2Rate constants from three compartment modeling of dynamic [¹⁸F]FDG PET in skeletal muscle in lean and obese subject during exercise plus insulin.

Lean Exercise + Insulin	V _b	k ₂ , (min ⁻¹)	K ₁ , (ml/ml/min)	k ₃ , (min ⁻¹)	K, (ml/ml/min)	DVCE, (ml/ml)	PF
1	0.032 (25)	0.767 (79)	0.084 (36)	0.458 (33)	0.031 (6)	0.110 (45)	0.374 (35)
2	0.015 (29)	0.672 (76)	0.089 (27)	0.531 (36)	0.039 (4)	0.133 (51)	0.441 (26)
3	0.024 (98)	-	0.258 (146)	0.601 (42)	0.024 (4)	0.044 (27)	0.092 (148)
4	0.042 (8)	≅ 0	0.058 (4)	0.251 (95)	0.058 (5)	-	1 (8)
5	0.043 (9)	0.017 (223)	0.076 (8)	0.111 (227)	0.066 (9)	4.4 (217)	0.865 (9)
6	0.039 (8)	≅ 0	0.030 (10)	0.901 (56)	0.030 (4)	-	1 (12)
7	0.017 (17)	0.724 (57)	0.072 (23)	0.458 (27)	0.028 (4)	0.099 (36)	0.387 (22)
8	0.022 (12)	0.554 (44)	0.049 (19)	0.279 (24)	0.017 (5)	0.090 (27)	0.335 (18)
9	0.040 (8)	0.294 (13)	0.026 (33)	0.346 (66)	0.014 (6)	0.088 (94)	0.540 (32)
10	0.044 (15)	0.162 (476)	0.060 (39)	0.834 (52)	0.050 (4)	0.370 (438)	0.837 (39)
11	0.024 (8)	≅ 0	0.025 (7)	0.633 (356)	0.025 (6)	-	1 (11)
12	0.054 (7)	≅ 0	0.029 (13)	1.05 (839)	0.029 (5)	-	1 (16)
Mean	0.033 *	0.602	0.055	0.518 †	0.034 *	0.094	0.707
± SD	0.012	0.19	0.024	0.23	0.013	0.03	0.288
Obese Exercise + Insulin	V _b	k ₂ , (min ⁻¹)	K ₁ , (ml/ml/min)	k ₃ , (min ⁻¹)	K, (ml/ml/min)	DVCE, (ml/ml)	PF
1	0.037 (8)	0.108 (74)	0.020 (17)	0.102 (59)	0.01 (10)	0.186 (58)	0.486 (15)
2	0.022 (8)	0.019 (138)	0.026 (7)	0.046 (237)	0.019 (36)	1.43 (132)	0.714 (32)
3	0.0014 (50)	0.338 (40)	0.033 (11)	0.283 (28)	0.015 (5)	0.099 (30)	0.455 (10)
4	0.026 (6)	0.039 (86)	0.0095 (12)	0.036 (159)	0.0046 (50)	0.246 (77)	0.480 (42)
5	-	≅ 0	0.052 (26)	0.35 (881)	0.052 (8)	-	1 (32)
6	≅ 0	-	0.107 (9)	0.236 (9)	0.0083 (4)	0.038 (7)	0.077 (9)
7	0.019 (23)	0.191 (62)	0.05 (16)	0.186 (41)	0.024 (6)	0.260 (48)	0.493 (15)
Mean	0.021	0.135	0.043	0.202	0.019	0.166	0.529
± SD	0.011	0.134	0.032	0.077	0.016	0.095	0.280

Values in parenthesis represent parameter precision expressed as a percent (%) coefficient of variation. K₁ and k₂ exchange parameters between plasma and intracellular space (free [¹⁸F]FDG pool); k₃ combined transport/phosphorylation parameter; V_b, fraction of total blood volume occupied by blood pool. K, fractional uptake of [¹⁸F]FDG; DVCE, distribution volume of free [¹⁸F]FDG; PF, phosphorylation fraction. Values in italic were excluded from the calculation of the group mean due to bad precision, as based on coefficient of variation > 100%.

* p < 0.05,

† p < 0.01. Unpaired Student t test. Lean vs obese.

TABLE 3Rate constants from three compartment modeling of dynamic [¹⁸F]FDG PET in skeletal muscle in lean and obese subject during rest plus insulin.

Lean Rest + Insulin	V _b	k ₂ , (min ⁻¹)	K ₁ , (ml/ml/min)	k ₃ , (min ⁻¹)	K, (ml/ml/min)	DVCE, (ml/ml)	PF
1	0.0145 (17)	0.322 (51)	0.035 (16)	0.226 (37)	0.015 (8)	0.111 (36)	0.413 (15)
2	0.010 (9)	0.013 (285)	0.011 (9)	0.089 (325)	0.0095 (15)	0.789 (279)	0.865 (12)
3	0.0037 (25)	0.344 (23)	0.024 (10)	0.088 (20)	0.0049 (9)	0.070 (14)	0.205 (11)
4	0.0055 (15)	0.009 (222)	0.028 (6)	0.057 (340)	0.024 (23)	2.93 (221)	0.856 (20)
5	0.024 (9)	≅ 0	0.031 (6)	0.551 (234)	0.031 (4)	-	1 (8)
6	0.016 (14)	0.228 (44)	0.035 (13)	0.16 (30)	0.014 (6)	0.154 (32)	0.413 (13)
7	≅ 0	2.44 (150)	0.073 (8)	0.485 (10)	0.012 (3)	0.03 (9)	0.166 (8)
8	≅ 0	0.165 (14)	0.023 (4)	0.042 (21)	0.0047 (10)	0.141 (11)	0.204 (9)
9	0.022 (10)	0.673 (25)	0.050 (15)	0.128 (15)	0.0080 (6)	0.075 (12)	0.159 (15)
10	0.005 (12)	0.042 (74)	0.012 (7)	0.076 (88)	0.0076 (12)	0.282 (68)	0.647 (10)
11	0.0082 (15)	0.559 (40)	0.036 (16)	0.282 (27)	0.012 (7)	0.065 (26)	0.335 (15)
12	0.0063 (15)	0.318 (42)	0.015 (15)	0.181 (30)	0.0056 (7)	0.049 (28)	0.363 (14)
Mean	0.011 †	0.331	0.031 †	0.185 *	0.012 *	0.108	0.469
± SD	0.007	0.204	0.017	0.135	0.007	0.077	0.249
Obese Rest + Insulin	V _b	k ₂ , (min ⁻¹)	K ₁ , (ml/ml/min)	k ₃ , (min ⁻¹)	K, (ml/ml/min)	DVCE, (ml/ml)	PF
1	≅ 0	0.166 (14)	0.015 (4)	0.037 (24)	0.0027 (12)	0.090 (11)	0.185 (11)
2	0.0064 (13)	0.169 (32)	0.022 (9)	0.099 (29)	0.0081 (7)	0.130 (25)	0.368 (9)
3	0.0015 (13)	≅ 0	0.0062 (3)	0.095 (538)	0.0062 (10)	0.121 (3)	1 (11)
4	0.0005 (33)	0.071 (21)	0.0067 (5)	0.005 (207)	0.0012 (17)	0.094 (18)	0.067 (175)
5	-	≅ 0	0.014 (13)	0.15 (165)	0.014 (11)	-	1 (22)
6	0.0085 (7)	0.116 (27)	0.012 (8)	0.034 (40)	0.0028 (18)	0.106 (20)	0.227 (15)
7	0.0064 (10)	0.006 (288)	0.008 (8)	0.013 (146)	0.005 (378)	-	0.685 (373)
Mean	0.0039	0.131	0.012	0.057	0.0058	0.108	0.556
± SD	0.0036	0.046	0.0056	0.036	0.0047	0.017	0.41

See legend in Table 2.

* p < 0.05,

† p < 0.01. Unpaired Student t test. Lean vs obese subjects